Molecular Catalysis 443 (2017) 60–68

Contents lists available at ScienceDirect

Molecular Catalysis

journal homepage: www.elsevier.com/locate/mcat

MCAT

Research Paper

$Pd_{0.09}Ce_{0.91}O_{2-\delta}$: A sustainable ionic solid-solution precatalyst for heterogeneous, ligand free Heck coupling reactions

Philani P. Mpungose, Neo I. Sehloko, Venkata D.B.C. Dasireddy, Narayanappa Mahadevaiah, Glenn E. Maguire, Holger B. Friedrich*

School of Chemistry and Physics, University of KwaZulu-Natal, Private Bag X54001, Durban 4001, South Africa

ARTICLE INFO

Article history:
Received 2 May 2017
Received in revised form
18 September 2017
Accepted 20 September 2017

Keywords:
Pd^{2+} substituted ceria
Solution combustion
Nanoparticles
Heck coupling reaction

ABSTRACT

A quick and easy method for the preparation of Pd^{2+} metal ion substituted in ceria, $Pd_{0.09}Ce_{0.91}O_{2-\delta}$ solid solution oxide, is described. The $Pd_{0.09}Ce_{0.91}O_{2-\delta}$ solid solution oxide was fully characterized by XRD, ICP-OES, BET, XPS, SEM, EDX, TEM, TGA and Raman spectroscopy. All characterization techniques strongly suggested that Pd^{2+} was successfully incorporated into the lattice structure of ceria. The effect of the reaction conditions on the catalytic properties of the $Pd_{0.09}Ce_{0.91}O_{2-\delta}$ solid solution catalyst initially was studied in detail with the model Heck reaction of iodobenzene and methylacrylate to obtain optimum reaction conditions. The $Pd_{0.09}Ce_{0.91}O_{2-\delta}$ solid solution catalyst then afforded substituted alkenes in good to excellent yields under these optimum reaction conditions. Steric and electronic effects were also studied, and were found to influence the catalytic activity. Characterization of the used catalyst suggests that Pd^{2+} in $Pd_{0.09}Ce_{0.91}O_{2-\delta}$ is reduced *in situ* to Pd^0 when employed in the Heck cross-coupling reactions. The catalyst was easily recovered by centrifuge and reused three times without significant loss of catalytic efficiency.

1. Introduction

Palladium catalysed Heck coupling reactions are a well-known and a well-established technique in organic chemistry and the pharmaceutical industry [1]. The Heck coupling reaction is now considered to be one of the most useful and practical tools in modern organic synthesis [2]. It involves the construction of a carbon-carbon (C—C) bond through a chemical reaction between an unsaturated halide and an alkene in the presence of a base and a palladium catalyst to form substituted alkenes [3,4]. These C—C bonds are of great importance in organic chemistry and are essential for all life on earth [5–10]. Several reviews have been published [11–16].

The most common catalytic systems used for Heck coupling reactions involve homogenous palladium-phosphine complexes, such as $PdCl_2(PPh_3)_2$ or $Pd(PPh_3)_4$, in the presence of a base [11–18]. Many ligands and catalysts have also been reported, but they are largely not available commercially and do not find extensive use [19,20]. This is mostly because the phosphine ligands are oxygen sensitive (easily oxidized) [17]. Furthermore, the efficient separation and subsequent recycling of homogenous palladium catalysts and ligand remains a challenge and an aspect of economic relevance [19,20].

As a result, the use of ligand-free heterogeneous palladium catalyst is often desirable because it permits easy handling, simple recovery and recyclability of the palladium catalyst. The increasing number of reports indicates that there is a growing interest in finding heterogeneous variants of Heck coupling reactions [6,7,20–26]. Most classes of heterogeneous catalysts described in literature involve immobilization of homogeneous Pd containing catalysts onto insoluble polymeric supports or solid inorganic supports. Frequently used supports are activated carbon [7], molecular sieves [27], metal oxides [8–10,28,29] and polymers [30,31].

Heterogeneous catalysis with the noble metal ion substituted in solid-state materials, such as in simple and complex oxides, is not well understood [32–34]. However, some authors of the present work have published some papers addressing the synthesis and catalytic behavior of binary oxide-based compounds substituted with noble metal ions to make ionic catalysts [35–37]. Hedge and co-workers have also published numerous papers addressing solution combustion synthesis and application of noble metal ionic catalysts [38–50]. All reports have shown that substitution of Pd^{2+} ions within the CeO_2 lattice allows for complete palladium dispersion,

* Corresponding author.
E-mail addresses: friedric@ukzn.ac.za, holgerbfriedrich@gmail.com (H.B. Friedrich).

http://dx.doi.org/10.1016/j.mcat.2017.09.022
2468-8231/

which, as a result, increases the activity of the ceria-based catalysts [38,51].

However, the 2 mol% level of Pd substitution usually investigated for these materials is at the detection limit of phase identification by conventional powder X-ray diffraction [51]. Thus, in most cases it is unclear whether the Pd is incorporated into the lattice structure of CeO_2 or is deposited on the surface of CeO_2 as PdO [51]. In this regard, we thought it would be worthwhile to prepare, and evaluate the phase composition and physicochemical properties of, a higher Pd-substituted $Pd_xCe_{1-x}O_{2-\delta}$ (9 mol% Pd) solid solution oxide by solution combustion. This ionic $Pd_{0.09}Ce_{0.91}O_{2-\delta}$ solid solution oxide was then tested on Heck cross coupling reactions. Using an air, moisture and thermally stable heterogeneous $Pd_{0.09}Ce_{0.91}O_{2-\delta}$ solid solution catalyst should offer simplicity of workup, recyclability and minimization of metallic waste. It should also offer higher turnover numbers since complete dispersion is achieved in similar Pd^{2+} ion substituted CeO_2 materials [38].

2. Experimental

2.1. Catalyst synthesis

Cerium ammonium nitrate [$(NH_3)Ce(NO_3)_6$, 99.9%], palladium chloride [$PdCl_2$, anhydrous, 60% Pd basis], urea [CH_4N_2O, 99.9%] were obtained from Sigma-Aldrich and were used without further purification.

2.1.1. Solution combustion synthesis of the $Pd_{0.09}Ce_{0.91}O_{2-\delta}$ oxide

The following materials were synthesized using an adaptation of a reported procedure [36]. For the synthesis of $Pd_{0.09}Ce_{0.91}O_{2-\delta}$ (6.7 wt% Pd), 2 mmol of $PdCl_2$ were dissolved in 10 mL of HCl (32%) in a borosilicate dish, and once all the $PdCl_2$ had dissolved, 40 mL of deionized water, 18 mmol of $(NH_3)Ce(NO_3)_6$, and 72 mmol CH_4N_2O (urea) were added. The solution was stirred at 100 °C to evaporate water and form a gel. The formed gel was introduced into a muffle furnace pre-heated to 120 °C, the furnace temperature was then increased gradually to 600 °C over 30 min, and maintained at that temperature for 5 h. A dark brown solid product was obtained. For the synthesis of blank CeO_2, the above procedure was followed without the addition of $PdCl_2$.

2.2. Catalyst characterization

A Bruker D8 Advance diffractometer, equipped with an XRK900 *in situ* cell and a Cu Kα source (λ = 1.5406 Å) was used to record the powder X-ray diffraction patterns of the samples. The structures were refined by the Rietveld method using the Full Prof Suite-2000 program. The average crystallite size (D) and lattice strain (ε) of CeO_2 and $Pd_{0.09}Ce_{0.91}O_{2-\delta}$ were estimated from the modified Rietveld method and Williamson-Hall (W-H) plots (1).

$$\beta_{hkl}\cos\theta = \frac{K\lambda}{D} + 4\varepsilon\sin\theta \quad (1)$$

X-ray photoelectron spectra (XPS) were recorded with a Thermo Scientific Multilab 2000 spectrometer equipped with the Al Kα radiation source (1486.6 eV). All the binding energies were referenced to the C(1s) peak (284.5 eV).

ICP-OES was performed using a Perkin Elmer Optical Emission Spectrometer Optima 5300 DV. The standards (1000 ppm Ce and Pd) were purchased from Fluka.

Raman spectroscopy was carried out using an Advanced 532 series spectrometer (NIR Spectrometer) utilizing Nuspec software, equipped with a visible laser of 514 nm.

Brunauer–Emmett–Teller (BET) surface area measurements were determined using a MicroMetrics TriStar 3000 porosimeter with N_2 as probe gas. About 0.4 g of each powder sample was degased overnight at 200 °C using a Micromeritics FlowPep 060 instrument prior to analysis.

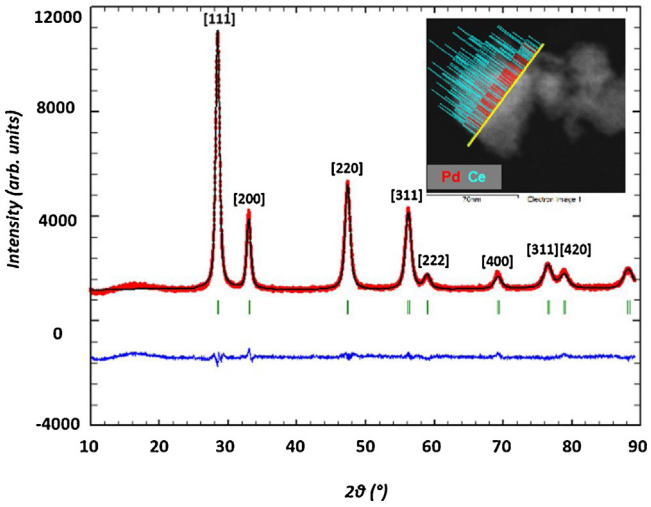

Fig. 1. Rietveld refined XRD pattern of $Pd_{0.09}Ce_{0.91}O_{2-\delta}$ and its STEM-EDX image (insert).

SEM images and EDX data were obtained with a Jeol JSM-6100 scanning microscope using a Bruker signal processing unit detector. The analysis was performed at random points along the surface of the catalyst. The samples were first mounted on aluminium stubs using double-sided carbon tape; they were then coated with gold using a Polaron E5100 coating unit.

For TEM analysis, the samples were viewed on Joel JEM-1010 Electron Microscope. For high resolution TEM (HR-TEM) and scanning electron microscopy (STEM) analysis, the samples were viewed on Joel JEM-2100 Electron Microscope and the images captured were analysed using iTEM software. The powder samples were ultrasonically dispersed in ethanol and supported on a perforated carbon film mounted on a copper grid prior to analysis.

TGA analysis was conducted with a TA SDT Q600 instrument under nitrogen flowing at 50 mL/min and at a temperature ramp rate of 10 °C/min from room temperature up to 1000° C with ca. 10 mg of sample.

2.3. General procedure for Heck cross-coupling reactions

A dry two-necked pear-shaped flask, equipped with a condenser containing a stirrer bar and 3 mL of DMF was charged with the aryl halide (2 mmol), olefin (1.5 eq.), triethylamine (1.5 eq.) and catalyst $Pd_{0.09}Ce_{0.91}O_{2-\delta}$ (0.3 mol% Pd). The reaction mixture was heated and stirred at 130 °C. A GC/MS (PerkinElmer Inc.–Clarus 560 S GC/MS; PONA column: 50 m × 0.15 mm) was used for monitoring the progress of the reaction and for product identification. After the reaction had gone to completion, the reaction mixture was cooled to room temperature and filtered. The filtrate was extracted with ethyl acetate, hexane and brine (1:3:3). The organic layer was dried with sodium sulphate and the solvent was then evaporated under reduced pressure. The residue was finally purified by flash chromatography on silica gel using ethyl acetate as the eluent.

3. Results and discussion

3.1. Physicochemical properties investigation

The microstructural parameters of the $Pd_{0.09}Ce_{0.91}O_{2-\delta}$ sample were determined using Rietveld refinement; the experimental, calculated and difference curves were plotted and are shown in Fig. 1.

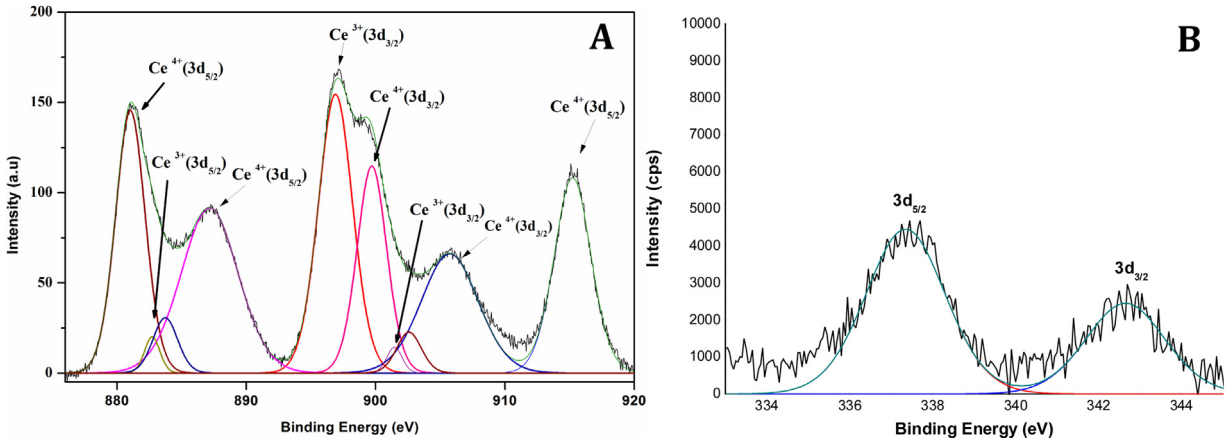

Fig. 2. Core level XPS of (A) Ce (3d) and (B) Pd (3d) in $Pd_{0.09}Ce_{0.91}O_{2-\delta}$ catalyst.

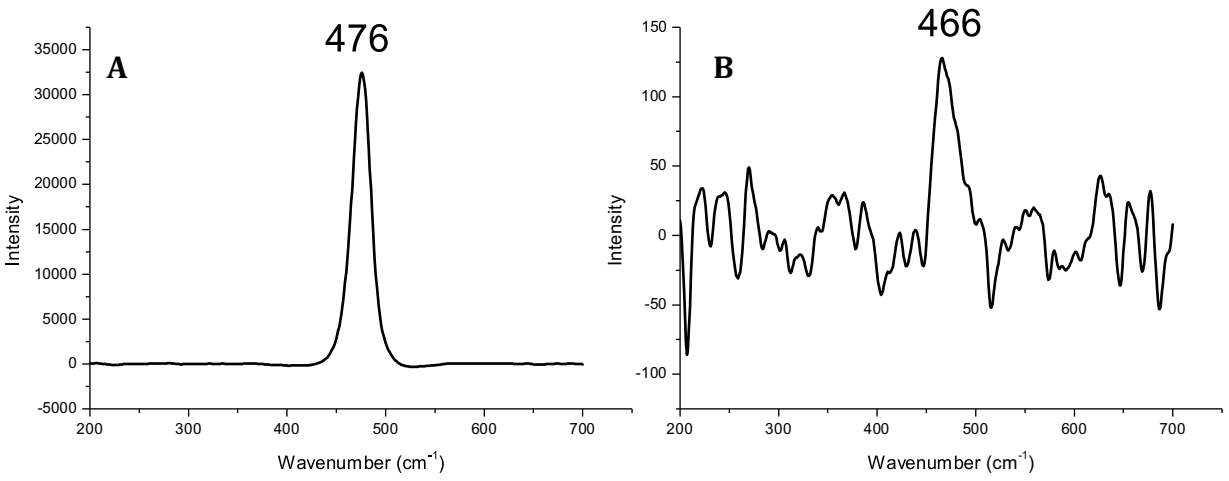

Fig. 3. Raman spectra of (a) CeO_2 and (b) $Pd_{0.09}Ce_{0.91}O_{2-\delta}$.

Table 1
Structural parameters of the investigated materials obtained from the XRD profiles.

	Rietveld refinement	Williamson-Hall method		TEM
	Lattice parameter a (Å)	Lattice strain ($\times 10^{-3}$)	Crystallite size (nm)	Average particle size (nm)
CeO_2	5.411(9)	0.9	19	22
$Pd_{0.09}Ce_{0.91}O_{2-\delta}$	5.424(9)	3	17	19

The observed peaks in the X-ray patterns of $Pd_{0.09}Ce_{0.91}O_{2-\delta}$ correspond only to the ceria phase with the fluorite structure (JCPDS 34-0394). The STEM-EDX (Fig. 1, insert) confirmed the presence of Pd and also shows that palladium is homogeneously dispersed in the ceria lattice.

The absence of the Pd^0 and/or PdO phase in the X-ray pattern of the $Pd_{0.09}Ce_{0.91}O_{2-\delta}$ sample suggests that the Pd^{2+} ions were successfully incorporated into the ceria lattice. The incorporation of the Pd^{2+} into the ceria lattice came with the expected physicochemical changes to ceria. The peak for the [111] plane shifts to lower 2 theta values upon the introduction of Pd^{2+} into the ceria lattice. The 2 theta value of the [111] plane shifts from 28.86° in pure CeO_2 to 28.83° in the $Pd_{0.09}Ce_{0.91}O_{2-\delta}$ sample. This shift is associated with increases in lattice parameters that cause the ceria lattice to be strained [51]. Table 1 shows that the lattice parameter *a* increases from 5.411(9) Å in CeO_2 to 5.424(9) Å in $Pd_{0.09}Ce_{0.91}O_{2-\delta}$. The XRD, XPS, ICP-OES, BET, SEM-EDS, TEM, TGA and Raman analyses for the CeO_2 sample are enclosed in the electronic supplementary information (ESI).

The Williamson-Hall plot was used to estimate the average crystallite size and lattice strain of the samples (Table 1). The $Pd_{0.09}Ce_{0.91}O_{2-\delta}$ sample showed about three times more lattice strain than pure ceria prepared by the same route (Table 1). The increased lattice strain in the $Pd_{0.09}Ce_{0.91}O_{2-\delta}$ sample indicates that lattice distortion occurs upon introduction of Pd^{2+} ions in the CeO_2 lattice [37,51]. The average crystallite size decreases slightly with the incorporation of the Pd^{2+} ions into the CeO_2 lattice. The average crystallite size of the blank CeO_2 is 19 nm, while that of $Pd_{0.09}Ce_{0.91}O_{2-\delta}$ decreased to 17 nm.

An assessment of recent reports on $Pd_xCe_{1-x}O_{2-\delta}$ solid solutions suggests that there is no conventional opinion to explain why the lattice parameter increases with the increasing concentration of Pd^{2+} ions [51]. We are of a view that the lattice parameters increase due to the formation of larger Ce^{3+} (1.23 Å) ions and the creation of more oxygen vacancies upon introduction of Pd^{2+} ions into the

ceria lattice. The increase in the lattice parameters then causes uniform lattice strain and a decrease in crystallite size. The formation of Ce^{3+} ions, that are larger than Ce^{4+} (0.97 Å) ions, was confirmed by XPS results (Fig. 2). The oxidation states of Pd and Ce in the $Pd_{0.09}Ce_{0.91}O_{2-\delta}$ catalyst were determined by XPS and core level XPS of Pd (3d) of $Pd_{0.09}Ce_{0.91}O_{2-\delta}$ as shown in Fig. 2. The Pd (3d) doublet lines were analysed to obtain the electronic state of palladium and the binding energy for Pd ($3d_{5/2}$) was found to be equal to 337.5 eV, which is typical for Pd^{2+} in the catalyst [37,51,52]. This main state of palladium was attributed to individual palladium ions localized in the ceria lattice of the $Pd_{0.09}Ce_{0.91}O_{2-\delta}$ solid solution oxide [51,53]. The elevated binding energy of the satellite peak at 342.5 eV further suggests that the palladium ions are localized in the ceria lattice.

Hence, the analysis of the Pd (3d) doublet lines strongly suggests that the environment of Pd^{2+} ions in the $Pd_{0.09}Ce_{0.91}O_{2-\delta}$ solid solution oxide is different from the oxygen environment in PdO, since the Pd ($3d_{5/2}$) line for PdO oxide is in the range of 336.7–337.0 eV [51,54]. The Ce^{4+} ($3d_{5/2}$) peak obtained at 881.5 eV is a characteristic of Ce^{4+} in CeO_2. Thus, partial filling of the valley between 881 eV and its satellite at 886 eV shows that Ce is in a mixed valence state (+4 and +3) since the Ce^{3+} (3d) in Ce_2O_3, is characterized by Ce^{3+} ($3d_{5/2}$) at 885.1 eV [52]. The ratios of oxidation states present in the catalyst were calculated as Ce^{4+}:Ce^{3+} of 4:1. Core level XPS of Ce(3d) in CeO_2 is shown in the Electronic supplementary information (ESI Figure SI2). The Ce^{4+}($3d_{3/2}$) peak obtained at 882.5 eV is characteristic of Ce^{4+} in CeO_2.

Raman spectroscopy was employed to comparatively analyze the CeO_2 and $Pd_{0.09}Ce_{0.91}O_{2-\delta}$ samples and the results are shown in Fig. 3. The peak at 465–480 cm^{-1} corresponds to the F_{2g} vibrational mode of oxygen ions in the [CeO_8] cubic subunit of the CeO_2 structure [37,51]. In blank CeO_2 this peak appears at 476 cm^{-1}, while for $Pd_{0.09}Ce_{0.91}O_{2-\delta}$ it shifts to a lower wavenumber of 466 cm^{-1} (Fig. 3). The bands at ca. 550 and 650 cm^{-1}, which are weak for blank CeO_2 and more intense for the $Pd_{0.09}Ce_{0.91}O_{2-\delta}$ sample, are assigned to the defect-induced vibrational mode (D-mode) [37,51]. The absence of a PdO peak (≈660 cm^{-1}) in the $Pd_{0.09}Ce_{0.91}O_{2-\delta}$ sample further suggests that the Pd^{2+} ions are fully dispersed in the lattice of CeO_2 and not deposited as PdO on its surface (ESI Figure SI5).

The Thermogravimetric analysis (TGA) (Fig. 4, solid lines) and differential thermal analysis (DTA) curves (Fig. 4, dotted lines) of

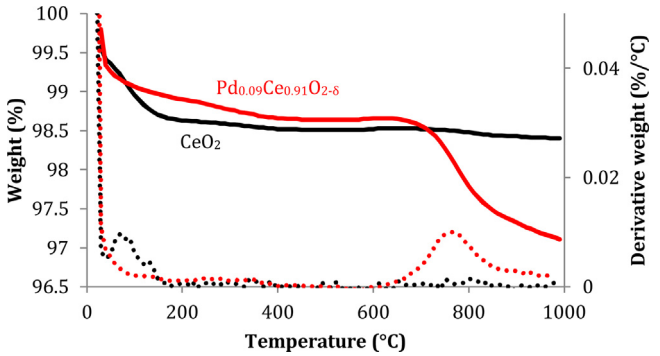

Fig. 4. TGA and DTA analysis of the investigated materials; (black) CeO_2 and (red) $Pd_{0.09}Ce_{0.91}O_{2-\delta}$. (For interpretation of the references to colour in this figure legend, the reader is referred to the web version of this article.)

the CeO_2 and $Pd_{0.09}Ce_{0.91}O_{2-\delta}$ samples are shown in Fig. 4. The two samples show an initial weight loss is the temperature range of 30–150 °C. Powdered CeO_2 is known to be slightly hydroscopic and it also absorbs small amount of carbon dioxide from the atmosphere. Thus, for the ceria samples, the weight loss observed below 150 °C can be attributed to both water and carbon dioxide loss. Furthermore, no weight loss was observed from 150 to 1000 °C in the ceria sample. For the $Pd_{0.09}Ce_{0.91}O_{2-\delta}$ sample, a second weight loss was observed at 760 °C (DTA) due to the thermal dissociation of the Pd-O bond to form metallic palladium [34,55]. Furthermore, the smooth nature of the weight loss change suggests that there are no intermediates formed before complete reduction to metallic palladium, implying that the reduction to the metallic state occurs in one step.

The elemental composition of the samples was analysed using EDS. The EDS spectrum of CeO_2 shows the presence of three elements; cerium, oxygen and chlorine (from HCl), while the EDS spectrum of the $Pd_{0.09}Ce_{0.91}O_{2-\delta}$ sample shows the presence of palladium in addition to the other three elements (Fig. 5). The SEM images of CeO_2 and $Pd_{0.09}Ce_{0.91}O_{2-\delta}$ samples have very similar surface morphology (Fig. 5). In both samples, the particles are present in the form of different sized lumps or flakes with round-shaped structures. These types of structures are generated due to the nature of the solution combustion synthesis method, where gases escape

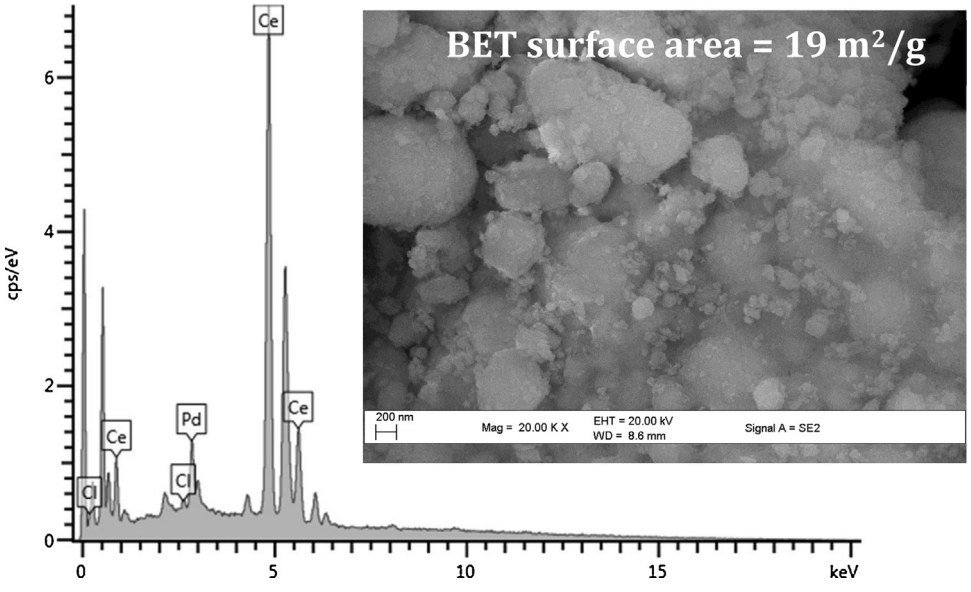

Fig. 5. SEM/EDX of $Pd_{0.09}Ce_{0.91}O_{2-\delta}$.

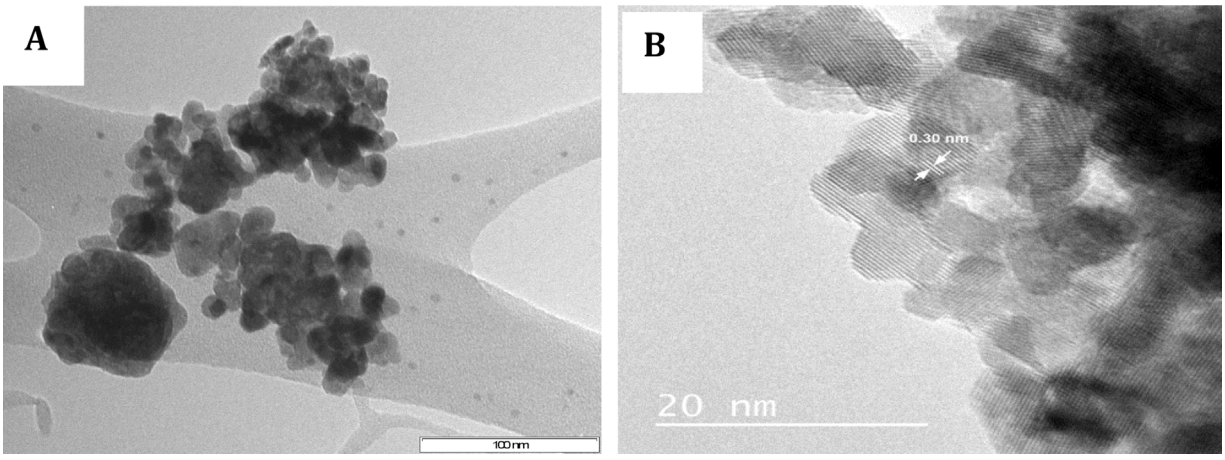

Fig. 6. (A) TEM (B) HR-TEM images of $Pd_{0.09}Ce_{0.91}O_{2-\delta}$.

Table 2
Optimisation of reaction conditions for Heck coupling reactions (the bold values are the chosen values).

Reaction parameters	
Reaction temperature	25, 80 and **130** °C
Solvent	Anisole, benzonitrile, **DMF**, DMSO, toluene, water and xylene
Base	K_2CO_3 and $(\mathbf{CH_3CH_3})_3\mathbf{N}$
Olefin equivalence	1, **1.5** and 2
Catalyst loading (based on Pd)	0.05, 0.1, **0.3**, 0.5 and 1 mol%

giving rise to porosity. The BET surface area of the $Pd_{0.09}Ce_{0.91}O_{2-\delta}$ sample was found to be 19 m^2/g.

Fig. 6A shows the TEM image of the $Pd_{0.09}Ce_{0.91}O_{2-\delta}$ sample with average particle size 19 nm. These particles are spherical in shape. No particles associated with PdO or Pd nanoparticles were observed in the $Pd_{0.09}Ce_{0.91}O_{2-\delta}$ TEM images. Qiao et al. and other researchers have reported Pd particles as cubic and rectangular shaped particles [56–59]. Hence, the absence of these cubic and rectangular shaped particles in the $Pd_{0.09}Ce_{0.91}O_{2-\delta}$ sample further suggests that Pd^{2+} ions are substituted into the lattice structure of CeO_2, and are not supported on the surface of CeO_2 as PdO.

The HR-TEM image of the solution combustion synthesized $Pd_{0.09}Ce_{0.91}O_{2-\delta}$ sample show lattice fringes of 0.30 nm (Fig. 6B). There were no lattice fringes associated with PdO or Pd nanoparticles observed [60]. Again, the absence of PdO lattice fringes and the presence of peaks due to Pd in the EDS spectrum (Fig. 5) of the $Pd_{0.09}Ce_{0.91}O_{2-\delta}$ sample further indicates that the Pd^{2+} ions are completely substituted into the CeO_2 lattice.

3.2. Catalyst activity investigation

To establish efficient Heck coupling conditions for the $Pd_{0.09}Ce_{0.91}O_{2-\delta}$ catalyst, methylacrylate and iodobenzene were used as model coupling partners. With this catalyst, neither copper salts nor activating ligands were necessary. In fact, addition of triphenylphosphine inhibited the reactions (ESI Table SI5). The effect of each reaction parameter was then investigated and the optimum reaction conditions are highlighted in Table 2. Excellent yields were only obtained with polar aprotic solvents (DMF, benzonitrile and DMSO) and DMF was chosen as the solvent in further studies since it allowed easier product isolation. The reactions were more rapid at 130 °C and 1.5 olefin equivalence was found to be the optimum olefin loading. Potassium carbonate and triethylamine gave comparable yields, however, triethylamine was chosen as the base in further studies because it simplifies catalyst recovery. K_2CO_3 requires successive washes with water to remove it from the recovered catalyst. It was also found that for the model coupling partners, complete iodobenzene conversion was achieved in two hours with catalyst loading as low as 0.05 mol% (based on Pd). However, a 0.3 mol% loading was chosen for further studies to allow shorter reaction times for less reactive coupling partners. Further catalyst testing was carried out under the reaction conditions highlighted in bold in Table 2.

A wide range of olefins and aryl halides were then tested to investigate group tolerance, steric and electronic effects under optimum reaction conditions using $Pd_{0.09}Ce_{0.91}O_{2-\delta}$ as a catalyst. It is

Table 3
Investigation of electronic effects and functional group tolerances of functionalised olefins.

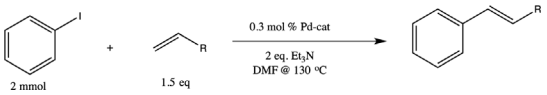

Entry	Alkene	Reaction time (h)	Isolated yield (trans) (%)	TON
1		1	90	300
2	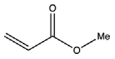	1	95	317
3	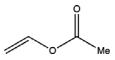	24	75	250
4		1	96	320
5		1	79	263
6		2	78	260
7	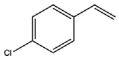	2	89	297
8	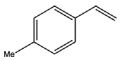	24	90	300
9	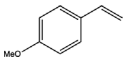	24	92	307
10		1	90	300

Table 4
Investigation of steric effects on the Heck coupling reactions.

Entry	Alkene	Reaction time (h)	Isolated yield (trans) (%)	TON
1	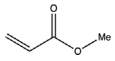	1	95	317
2	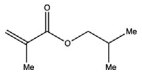	12	97	323
3	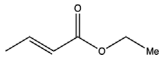	70	96	320

Table 5
Investigating the effect of varying the aryl iodide on the Heck coupling reactions.

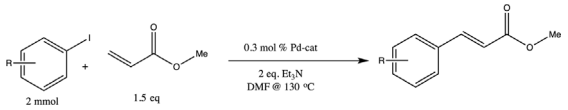

Entry	R	Reaction time (h)	Isolated yield (% trans)	TON
1	H	1	95	317
2	4-OH	2	75	250
3	4-CH_3	1	98	327
4	3-CH_3	3	96	320
5	4-NH_2	2	95	317
6	3-NH_2	4	92	307
7	4-$COCH_3$	2	90	300
8	3-$COCH_3$	2	94	313
9	4-NO_2	30	71	237
10	3-NO_2	7	75	250
11	3-CF_3	2	93	310

reported that both steric and electronic factors can favour arylation at the terminal position of the olefin or on the more exposed carbon [3,61,62]. Two sets of experiments were carried out to learn more about the catalyst activity. First, the olefins were varied and the aryl halide was kept constant as iodobenzene (Tables 3 and 4). Secondly, the aryl halides were varied and the olefin was kept constant as methylacrylate (Table 5).

Aliphatic and aromatic olefins with electron withdrawing and donating group were arylated with iodobenzene and the results are tabulated in Table 3. Entries 1–5 in Table 3 are of aliphatic olefins with varying functional groups. It was observed that olefins with electron withdrawing groups are easily arylated (Entries 1, 2, 4 and 5), with reaction times of less than an hour. However, Entry 3, which shows an olefin with an electron-donating group, has a longer reaction time. Entries 6–10 show the arylation of various styrene derivatives. The arylation of styrene (Entry 6) goes to completion in 2 h, however, three products formed; predominantly *trans*-stilbene (78%), and *cis*-stilbene (19%) and 1,1-diphenylethene as minor products. These side products were not observed in the arylation of other styrene derivatives. The styrene derivative with a methyl or methoxy group as a substituent took longer to go to completion (Table 3, Entries 8, 9). This further confirms that electron donating substituents on olefins slow down the reaction. Hence, the electronic effect controls the catalyst activity for both cyclic and acyclic olefins.

To investigate any possible steric effects, the reactivity of methylacrylate, ethyl crotonate and isobutylmethacrylate with iodobenzene was monitored (Table 4). It was found that steric effects play a major role in the catalysis. Thus, the reaction with methyacrylate went to completion in an hour, while it took 12 and 70 h for isobutylmethacrylate and ethyl crotonate to react to completion, respectively. Isobutylmethacrylate (Table 4, Entry 2) has a 1,1 disubstitution and ethyl crotonate (Table 4, Entry 3) is 1,2-disubstituted. Thus, isobutylmethacrylate has a more exposed carbon-carbon double bond than ethyl crotonate, and hence it reacts faster. In conclusion, the Heck cross coupling reactions favour electron deficient and less hindered (less substituted) olefins.

The scope of reactivity of various aryl halides was then investigated. It was found that aryl bromides and chlorides do not react under our optimum conditions. Various aryl iodides were then investigated to gain better understanding of the catalyst activity. With aryl iodides, both the electronic effect and substituent position effect were explored (Table 5). We found that most aryl iodides gave comparative reaction times; the electronic effect did not greatly influence the reactions (with an exception of iodonitrobenzenes). It was also observed that the position of the substituent on the aryl iodide has some influence in the reaction rate. Thus, Entries 3–4 show that the position of the methyl group influences the arylation rate of iodotoluene in that 4-iodotoluene is more reactive than 3-iodotoluene. The substituent position effect is more pronounced in Entries 9–10. In this case, 4-nitroiodobenzene is far less reactive than 3-nitroiodobenzene. It is unclear at this point how the substituents on aryl iodides affect the reactivity of the catalyst, however, the initial observation is that electron rich aryliodides are coupled more efficiently to methyl acrylate than to electron deficient aryliodides. This is discussed further in the reaction mechanism section.

The product yield (stilbene) of the present catalytic system was compared to other heterogeneous, ligand-free palladium catalysed Heck coupling reactions reported in literature (Table 6) [63–66]. The stilbene yield in this work was found to be comparable to those obtained by Nasrollahzadeh et al., Sanjaykmar et al. and Monopoli et al. [19,64,66]. However, the present catalyst system gives better results than those reported by Perosa et al. and Karami et al. [63,65].

3.3. Catalyst recovery, recyclability and leaching investigations

3.3.1. Used catalyst characterisation

The EDS spectrum of the used catalyst shows that it still contains palladium (Fig. 7). It further indicated that the surface concentra-

Table 6
Performance comparison of the present catalyst in Heck cross coupling reactions of iodobenzene and styrene against other related heterogeneous catalysts.

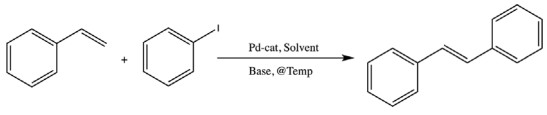

Entry	Catalyst	Reaction conditions	Time/h	Yield/%	[Ref.]
1	Pd/C 5% (0.05 mol% Pd)	Isooctane, H_2O, Aliquant 336, 100 °C	20	46	[63]
2	Pd-NPs/ZrO_2 (0.3 mol% Pd)	H_2O, TBAOH, 90 °C	4	81	[64]
3	Pd-complex/TiO_2 (0.12 mol% Pd)	MeOH, Na_2CO_3, 65 °C	7	30	[65]
4	$Ce_{0.98}Pd_{0.02}O_{2-\delta}$ (1.52 mol% Pd)	DMF, K_2CO_3, 130 °C	6	64	[66]
5	TiO_2@Pd (1 mol%)	DMF, $(CH_3CH_2)_3N$, 140 °C	10	93	[19]
6	$Pd_{0.09}Ce_{0.91}O_{2-\delta}$ (0.3 mol% Pd)	DMF, $(CH_3CH_2)_3N$, 130 °C	2	78	This paper

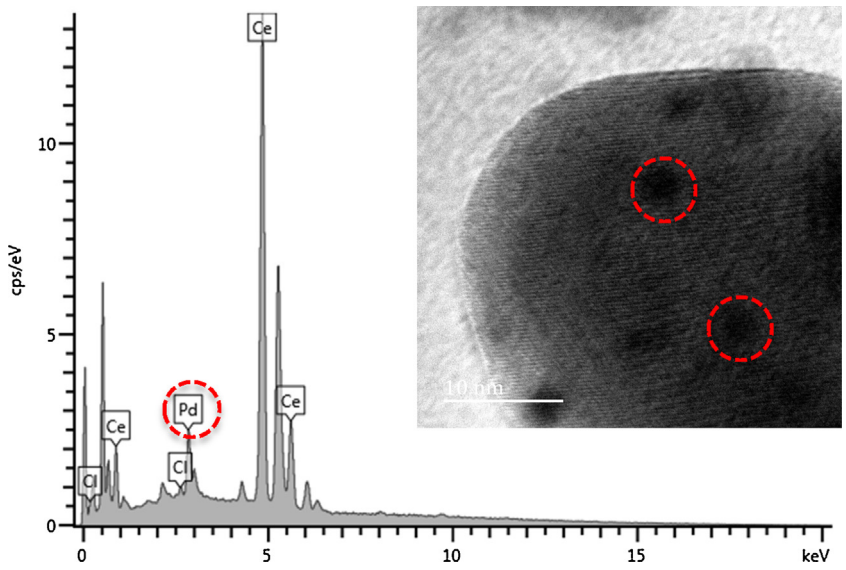

Fig. 7. The EDS spectrum and TEM image (insert) of the recovered catalyst.

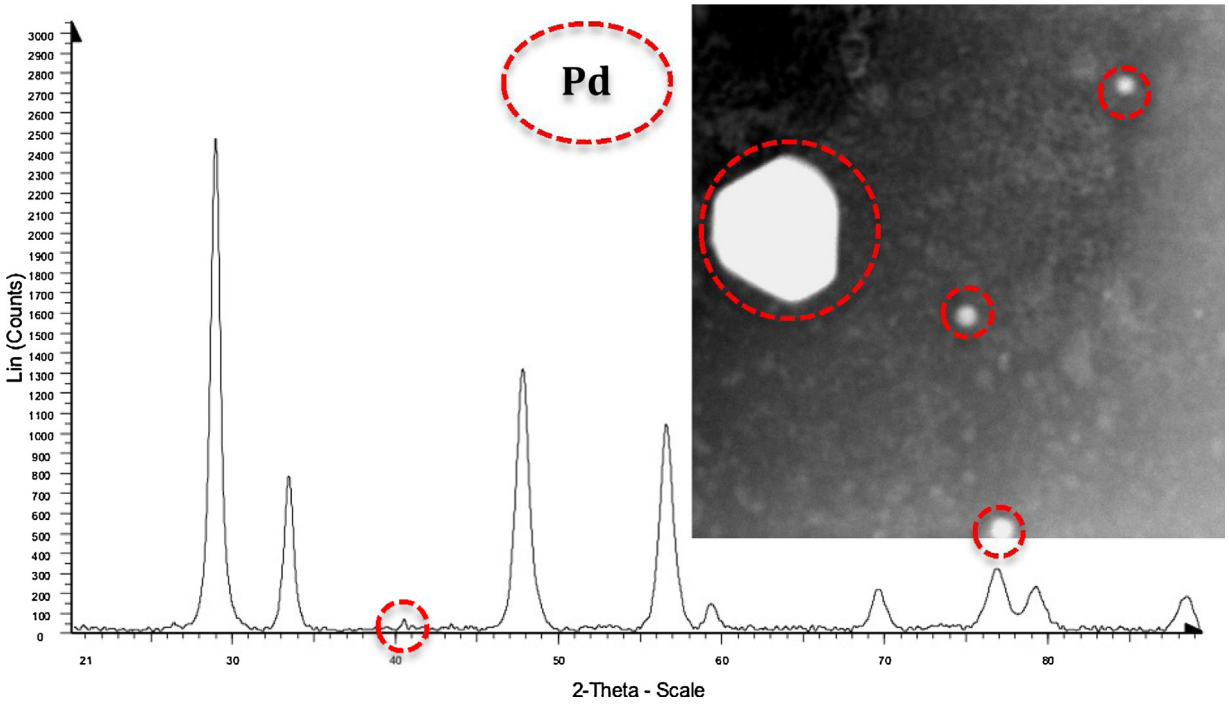

Fig. 8. The XRD pattern and STEM image (insert) of the recovered catalyst.

tion of palladium in the used catalyst is not significantly different to that of the fresh catalyst. The TEM image of the used catalyst shows the presence of palladium nanoparticles on the surface of ceria, this indicates that palladium ions are extruded from the lattice of ceria during the reaction (Fig. 7, insert).

The XRD pattern of the recovered catalyst also shows that the fluorite structure of the catalyst was intact; however, there is a small peak at 40° 2-θ, indicating the presence of Pd^0. This further suggests that Pd^{2+} ions are extruded from the lattice of ceria and sit on the surface as palladium nanoparticles (Fig. 8). In addition, the STEM images of the used catalyst also show Pd^0 particles deposited on ceria (Fig. 8, insert). This thus suggests that the single phase $Pd^{2+}_{0.09}Ce_{0.91}O_{2-\delta}$ solid solution is not the active species and that catalysis occurs instead over the reduced two phase Pd^0/CeO_2. Misch et al. reported similar observations for $Ce_{1-x}Pd_xO_{2-\delta}$ catalysed C—H bond activation [33]. In their system, the $Ce_{1-x}Pd_xO_{2-\delta}$ material did not become active until it was significantly reduced by ethylene and hydrogen flowing over the catalyst.

3.3.2. Catalyst leaching and recyclability tests

A mixture of $Pd_{0.09}Ce_{0.91}O_{2-\delta}$, iodobenzene, methylacrylate and triethylamine in DMF was stirred for an hour at 130 °C. After completion of the reaction, the catalyst was separated by centrifuge. (a) The mother liquor was analysed by ICP-OES for palladium content. (b) To the recovered catalyst, fresh substrates were added, namely iodobenzene, methylacrylate, triethylamine, and stirred in DMF at 130 °C for an hour. After completion of the reaction, the catalyst was separated by centrifuge, and parts (a) and (b) were repeated. This process was repeated three times and the results are tabulated in Table 7.

Table 7
Leaching and recyclability test[a].

	Reaction time/h	% Conversion	Amount Pd leached (ICP)/ppm
Cycle 1	1	100	0.35
Cycle 2	1	98	0.35
Cycle 3	1	98	0.25

[a] Pd content in fresh catalyst = 390 ppm.

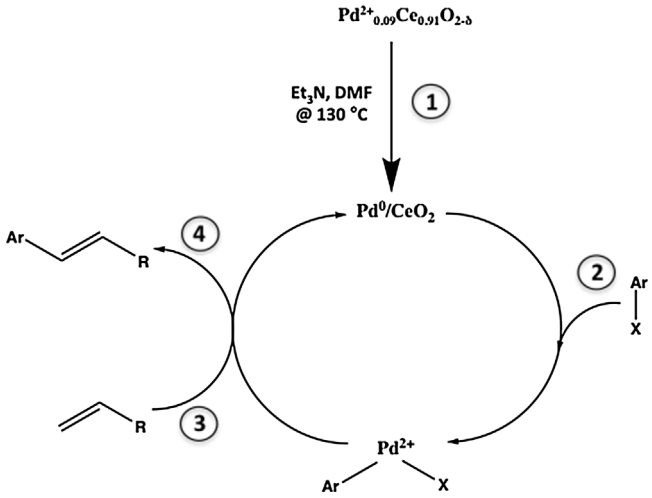

Scheme 1. Proposed Heck coupling reaction mechanism catalysed by the $Pd_{0.09}Ce_{0.91}O_{2-\delta}$ precatalyst.

The catalyst was recycled successfully three times without any significant loss in activity. However, the ICP results show that there was a minimal metal contamination of the products; a total of about 0.25% of palladium leached out of the $Pd_{0.09}Ce_{0.91}O_{2-\delta}$ solid solution over the three cycles. When the filtrate from cycle one was stirred with methylacrylate and 3-iodoacetophenone only 15% conversion was achieved in two hours, as compared to 100% conversion with the fresh catalyst. This implies that the reaction mechanism of the filtrate is different to that of the fresh catalyst. Although these results suggest that the $Pd_{0.09}Ce_{0.91}O_{2-\delta}$ catalysed Heck coupling reactions are largely heterogeneous, reports in literature have shown that supported palladium catalyst are mostly reservoirs of active soluble zerovalent palladium species [2,67–70]. Thus there is a possibility of a dissolution-recapture mechanism, with ceria acting like a Pd^0 scavenger. In any case, the $Pd_{0.09}Ce_{0.91}O_{2-\delta}$ precatalyst has proven effective in minimisation of metallic waste and allows for simplification of work-up.

3.4. Proposed mechanism

There are two main proposed mechanisms for the palladium catalysed Heck coupling reaction using homogeneous catalysts, namely the Pd^0/Pd^{2+} and Pd^{2+}/Pd^{4+} catalytic cycles. For the heterogeneous Heck reaction discussed here, the mechanism is not clear. However, the catalytic activity data and the physicochemical properties of the fresh and used catalyst suggest that the reaction follows a Pd^0/Pd^{2+} catalytic cycle (Scheme 1). The XRD diffractogram and HR-TEM images of the used catalyst suggest that palladium extrudes from the ceria lattice and is deposited as palladium nanoparticles on the surface of ceria. Hence, we proposed that the first step in the reaction mechanism is 'pre-activation' which allows $Pd^{2+}_{0.09}Ce_{0.91}O_{2-\delta}$ to enter the catalytic cycle as Pd^0/CeO_2 (**1**). The Pd^{2+} ions in the fresh catalyst are reduced *in situ* by DMF and/or triethylamine to Pd^0 [14,71,72]. Since Pd^0 is more electron rich than Pd^{2+}, it allows for oxidative addition of the aryl iodide, which marks the beginning of the catalytic cycle (**2**).

The olefin coordinates and forms a pi complex with palladium (**3**). The catalytic results suggest that this olefin insertion is likely the rate-determining step. The oxidative addition step cannot be the rate-limiting step, since varying aryl iodides gave comparable activity. Similar observations were reported by de Vries et al., who suggested that oxidative addition only becomes a rate determining step under ligand-free Heck coupling of aryl bromide [73]. Olefin insertion is then followed by β-hydride elimination, and the dissociation of the product moiety liberates the reaction product (**4**). The active catalyst is then regenerated through reductive elimination of hydrogen by the base triethylamine.

4. Conclusions

In conclusion, a more highly Pd substituted ceria catalyst (9 mol%), $Pd_{0.09}Ce_{0.91}O_{2-\delta}$ was prepared, characterized by various techniques and shown to be catalytically active towards the Heck coupling reaction between aryl iodides and alkenes. The physicochemical properties of this material indicate that the Pd^{2+} ions are substituted in the lattice structure of ceria and not deposited on its surface as PdO. However, used catalyst characterisation revealed that the catalysis occurs over the reduced two phase Pd^0/CeO_2 and not on the as prepared monophasic $Pd_{0.09}Ce_{0.91}O_{2-\delta}$. Good to excellent yields of substituted olefins were obtained with the $Pd_{0.09}Ce_{0.91}O_{2-\delta}$ precatalyst when tested on ligand-free Heck coupling reactions. The Heck reactions were also shown to be affected by electronic and steric effects. Electron deficient olefins react more rapidly compared to electron rich olefins. In addition, an olefin with a more exposed carbon-carbon double bond also reacts more rapidly. Finally, the active catalyst (Pd^0/CeO_2) can be easily recovered and reused for at least three times without any significant loss in efficiency and only a negligible amount of palladium was detected in the product solution (0.35 ppm).

Acknowledgements

We would like to express our gratitude to Mintek and the Department of Science and Technology, South Africa (Advanced Metals Initiative program) for financial support. The authors would also like to thank Dr M Shozi, Dr S Mohamed, Dr S Singh and the rest of the UKZN catalysis research group for helpful discussions.

Appendix A. Supplementary data

Supplementary data associated with this article can be found, in the online version, at http://dx.doi.org/10.1016/j.mcat.2017.09.022.

References

[1] J.C. Hierso, Angew. Chem. Int. Ed. 53 (2014) 920.
[2] A. Biffis, M. Zecca, M. Basato, J. Mol. Catal. A: Chem. 173 (2001) 249.
[3] R.F. Heck, J.P. Nolley, J. Org. Chem. 37 (1972) 2320.
[4] T. Mizoroki, K. Mori, A. Ozaki, Bull. Chem. Soc. Jpn. 44 (1971) 581.
[5] S. Sisodiya, L.R. Wallenberg, E. Lewin, O.F. Wendt, Appl. Catal. A: Gen. 503 (2015) 69.
[6] J. Xiao, Z. Lu, Y. Li, Ind. Eng. Chem. Res. 54 (2015) 790.
[7] X.U. Qijie, S.H.I. Wenzhong, Z.U.O. Chunshan, L.I.U. Dayong, Y.A.N.G. Chun, Z.H.A.O. Xiang, L.I.U. Pengcheng, Chin. J. Appl. Chem. 32 (2015) 428.
[8] C. Battilocchio, B.N. Bhawal, R. Chorghade, B.J. Deadman, J.M. Hawkins, S.V. Ley, Isr. J. Chem. 54 (2014) 371.
[9] M. Hosseini-Sarvari, Z. Razmi, M.M. Doroodmand, Appl. Catal. A: Gen. 475 (2014) 477.
[10] C. Pavia, F. Giacalone, L.A. Bivona, A.M.P. Salvo, C. Petrucci, G. Strappaveccia, L. Vaccaro, C. Aprile, M. Gruttadauria, J. Mol. Catal. A: Chem. 387 (2014) 57.
[11] A. de Meijere, F.E. Meyer, Angew. Chem. Int. Ed. 33 (1995) 2379.
[12] I.P. Beletskaya, A.V. Cheprakov, Chem. Rev. 100 (2000) 3009.

[13] D. Mc Cartney, P.J. Guiry, Chem. Soc. Rev. 40 (2011) 5122.
[14] L. Yin, J. Liebscher, Chem. Rev. 107 (2007) 133.
[15] K. Köhler, R.G. Heidenreich, J. Krauter, Chem. Eur. J. 8 (2002) 622.
[16] A. Kumbhar, Top. Curr. Chem. 375 (2016) 2.
[17] M. Islam, P. Mondal, K. Tuhina, A.S. Roy, J. Braz. Chem. Soc. 22 (2011) 319.
[18] H. Doucet, Angew. Chem. Int. Ed. 53 (2014) 629.
[19] M. Nasrollahzadeh, A. Azarian, A. Ehsani, M. Khalaj, J. Mol. Catal. A: Chem. 394 (2014) 205.
[20] A. Banazadeh, A. Pirisedigh, F. Aryanasab, H. Salimi, S. Shafiei-Haghighi, Inorg. Chim. Acta. 429 (2015) 132.
[21] J.W. Brown, N.N. Jarenwattananon, T. Otto, J.L. Wang, S. Gloggler, L. Bouchard, Catal. Commun. 65 (2015) 105.
[22] B. Movassagh, F.S. Parvis, M. Navidi, Appl. Organomet. Chem. 29 (2015) 40.
[23] A. Naghipour, A. Fakhri, Catal. Commun. 73 (2016) 39.
[24] S. Sobhani, Z.M. Falatooni, S. Asadi, M. Honarmand, Catal. Lett. 146 (2015) 255.
[25] S. Sobhani, Z. Zeraatkar, F. Zarifi, New J. Chem. 39 (2015) 7076.
[26] L. You, W. Zong, G. Xiong, F. Ding, S. Wang, B. Ren, I. Dragutan, V. Dragutan, Y. Sun, Appl. Catal. A: Gen. 511 (2016) 1.
[27] J. Demel, M. Lamac, J. Cejka, P. Stepnicka, ChemSusChem 2 (2009) 442.
[28] Z. Li, J. Chen, W. Su, M. Hong, J. Mol. Catal. A: Chem. 328 (2010) 93.
[29] A.R. Hajipour, N.S. Tadayoni, Z. Khorsandi, Appl. Organomet. Chem. 30 (2016) 590.
[30] N. Kann, Molecules 15 (2010) 6306.
[31] S.J. Tabatabaei Rezaei, A. Shamseddin, A. Ramazani, A. Mashhadi Malekzadeh, P. Azimzadeh Asiabi, Appl. Organomet. Chem. (2017) e3707.
[32] J.A. Kurzman, J. Li, T.D. Schladt, C.R. Parra, X. Ouyang, R. Davis, J.T. Miller, S.L. Scott, R. Seshadri, Inorg. Chem. 50 (2011) 8073.
[33] L.M. Misch, J.A. Kurzman, A.R. Derk, Y.I. Kim, R. Seshadri, H. Metiu, E.W. McFarland, G.D. Stucky, Chem. Mater. 23 (2011) 5432.
[34] J.A. Kurzman, L.M. Misch, R. Seshadri, Dalton Trans. 42 (2013) 14653.
[35] M. Narayanappa, V.D.B.C. Dasireddy, H.B. Friedrich, Appl. Catal. A: Gen. 135 (2012) 447.
[36] T. Cwele, N. Mahadevaiah, S. Singh, H.B. Friedrich, Appl. Catal. B: Environ. 182 (2016) 1.
[37] T. Cwele, N. Mahadevaiah, S. Singh, H.B. Friedrich, A.K. Yadav, S.N. Jha, D. Bhattacharyya, N.K. Sahoo, Catal. Sci. Tech. 6 (2016) 8104.
[38] M.S. Hegde, G. Madras, K.C. Patil, Acc. Chem. Res. 42 (2009) 704.
[39] T. Baidya, G. Dutta, M.S. Hegde, U.V. Waghmare, Dalton Trans. (2009) 455.
[40] A. Baidya, G. Deshpandey, M.S. Hegde, J. Phys. Chem. C 113 (2009) 4059.
[41] P. Bera, K.C. Patil, V. Jayaram, G.N. Subbanna, M.S. Hegde, J. Catal. 196 (2000) 293.
[42] P. Bera, K.R. Priolkar, P.R. Sarode, M.S. Hegde, S. Emura, R. Kumashiro, N.P. Lalla, Chem. Mater. 14 (2002) 3591.
[43] A. Gayen, K.R. Priolkar, P.R. Sarode, V. Jayaram, M.S. Hegde, G.N. Subbanna, S. Emura, Chem. Mater. 16 (2004) 2317.
[44] A. Gupta, A. Kumar, U.V. Waghmare, M.S. Hegde, Chem. Mater. 21 (2009) 4880.
[45] S. Roy, M.S. Hegde, Catal. Commun. 9 (2008) 811.
[46] S. Roy, A. Marimuthu, M.S. Hegde, G. Madras, Catal. Commun. 9 (2008) 101.
[47] P. Singh, M.S. Hegde, Dalton Trans. 39 (2010) 10768.
[48] P. Singh, M.S. Hegde, Chem. Mater. 21 (2009) 3337.
[49] P. Singh, M.S. Hegde, J. Gopalakrishnan, Chem. Mater. 20 (2008) 7268.
[50] K.C. Patil, M.S. Hegde, T. Rattan, S.T. Aruna, Chemistry of Nanocrystalline Oxide Materials: Combustion Synthesis, Properties and Applications; World Scientific: 5 Toh Tuck Link, Singapore, 2008, pp. 9–41.
[51] R.V. Gulyaev, T.Y. Kardash, S.E. Malykhin, O.A. Stonkus, A.S. Ivanova, A.I. Boronin, Phys. Chem. Chem. Phys. 16 (2014) 13523.
[52] R.V. Gulyaev, A.I. Stadnichenko, E.M. Slavinskaya, A.S. Ivanova, S.V. Koscheev, A.I. Boronin, Appl. Catal. A: Gen. 41 (2012) 439.
[53] K.R. Priolkar, P. Bera, P.R. Sarode, M.S. Hegde, S. Emura, R. Kumashiro, N.P. Lalla, Chem. Mater. 14 (2002) 2120.
[54] S. Colussi, A. Gayen, M. Farnesi Camellone, M. Boaro, J. Llorca, S. Fabris, A. Trovarelli, Angew. Chem. Int. Ed. 48 (2009) 8481.
[55] S. Hinokuma, H. Fujii, M. Okamoto, K. Ikeue, M. Machida, Chem. Mater. 22 (2010) 6183.
[56] Z.A. Qiao, Z. Wu, S. Dai, ChemSusChem 6 (2013) 1821.
[57] H. Zhang, M. Jin, Y. Xia, Angew. Chem. Int. Ed. 51 (2012) 7656.
[58] W. Niu, L. Zhang, G. Xu, Nanoscale 5 (2013) 3172.
[59] Y. Xia, Y. Xiong, B. Lim, S.E. Skrabalak, Angew. Chem. Int. Ed. 48 (2009) 60.
[60] C. Rossy, J. Majimel, M.T. Delapierre, E. Fouquet, F.X. Felpin, Appl. Catal. A: Gen. 482 (2014) 157.
[61] A. King, N. Yasuda, Organometallics in Process Chemistry, 6, Springer, Berlin Heidelberg, 2004, pp. p205.
[62] E. Mieczyńska, A. Gniewek, I. Pryjomska-Ray, A.M. Trzeciak, H. Grabowska, M.A. Zawadzki, Appl. Catal. A: Gen. 393 (2011) 195.
[63] A. Perosa, P. Tundo, M. Selva, S. Zinovyev, A. Testa, Org. Biomol. Chem. 2 (2004) 2249.
[64] A. Monopoli, A. Nacci, V. Calò, F. Ciminale, P. Cotugno, A. Mangone, L.C. Giannossa, P. Azzone, N. Cioffi, Molecules 15 (2010) 4511.
[65] K. Karami, M.B. Shehni, N. Rahimi, Appl. Organomet. Chem. 27 (2013) 437.
[66] S.R. Sanjaykumar, B. Mukri, S. Patil, G. Madras, M.S.J. Hegde, Chem. Sci. 123 (2011) 47.
[67] M. Bhanage, M. Shirai, Chem. Eur. J. 6 (2000) 843.
[68] P. Albers, J. Pietsch, S.F. Parker, J. Mol. Catal. A: Chem. 173 (2001) 275.
[69] J.A. Gladysz, Recoverable and Recyclable Catalysts, John Wiley & Sons, Ltd, Chichester UK, 2009, pp. 1–45.
[70] R.L. Augustine, S.T. O'Leary, J. Mol. Catal. A: Chem. 95 (1995) 277.
[71] A. Jutand, The Mizoroki-Heck Reaction, John Wiley & Sons, Ltd., Chichester, UK, 2009, pp. 6–50.
[72] J.P. Collman, R.G. Finke, J.R. Norton, Principles and Applications of Organotransition Metal Chemistry, 2nd ed., University Science Books, Mill Valley, California, 1987, pp. 1145–1146.
[73] A.H.M. de Vries, J.M.C.A. Mulders, J.H.M. Mommers, H.J.W. Henderickx, J.G. de Vries, Org. Lett. 5 (2003) 3285.